An Extension of the Lumped-Network FDTD Method to Linear Two-Port Lumped Circuits

Oscar González, José A. Pereda, *Member, IEEE*, Amparo Herrera, *Member, IEEE*, and Ángel Vegas, *Member, IEEE*

***Abstract*—The lumped-network finite-difference time-domain (LN-FDTD) technique is an extension of the conventional finite-difference time-domain (FDTD) method that allows the systematic incorporation of linear one-port lumped networks (LNs) into a single FDTD cell.**

This paper presents an extension of the LN-FDTD technique, which allows linear two-port (TP)-LNs to be incorporated into the FDTD framework. The method basically consists of describing a TP-LN by means of its admittance matrix in the Laplace domain. By applying the Mobius transformation technique, we then obtain the admittance matrix of the TP-LN in the Z-transform domain. Finally, appropriate digital signal-processing methodologies are used to derive a set of difference equations that models the TP-LN behavior in the discrete-time domain. These equations are solved in combination with the Maxwell–Ampère's equation.

To show the validity of the TP-LN-FDTD technique introduced here, we have considered the equivalent circuit of a chip capacitor and a linear circuit model of a generic metal–semiconductor field-effect transistor. These LNs have been placed on a microstrip gap and the scattering parameters of the resulting hybrid circuit have been computed. The results are compared with those obtained by using the electromagnetic simulator Agilent HFSS in combination with the circuital simulator ADS, and with those calculated by ADS alone. For the chip capacitor, experimental measurements have also been carried out. The agreement among all the simulated results is good. Generally speaking, the measured results agree with the simulated ones. The differences observed are mainly due to the influence of the subminiature A connectors and some mismatching at the ports.

***Index Terms*—Finite-difference time-domain (FDTD) methods, global modeling, lumped networks (LNs).**

I. Introduction

THE finite-difference time-domain (FDTD) method was originally introduced as a technique for the numerical analysis of electromagnetic field problems [1]. Over the last decade, a considerable effort has been made to incorporate lumped-circuit elements into the FDTD framework [2]–[7]. The resulting extended FDTD formulations are often referred to as the lumped-element (LE)-FDTD method. This method has allowed complex microwave and millimeter-wave circuits, including both distributed and lumped components, to be successfully analyzed.

The so-called lumped-network (LN)-FDTD method is an improvement of the LE-FDTD technique that allows a systematic and simple incorporation of linear one-port LNs into a single FDTD cell [8]. Over the last few years, the LN-FDTD method has received a great deal of attention. Several alternative discretization schemes, different to the one originally presented in [8], have been introduced [9]–[14]. Moreover, the LN-FDTD method has recently been extended to model nonlinear packaged Schottky diodes [15]–[18].

The LN-FDTD method may also be used to model two-port (TP) lumped circuits. However, this involves decomposing the circuit in its one-port (two-terminal) LN constituents, which reproduces the limitations encountered with the LE-FDTD method: the lack of uniqueness of the resulting circuit topology over the FDTD mesh, and the risk of losing the lumped nature of the circuit when several FDTD cells are needed for its implementation.

This paper introduces an extension of the LN-FDTD method to linear TP-LNs. In the following, we will refer to this technique as the TP-LN-FDTD method. The proposed approach comprises the following main steps.

Step 1) As a starting point, the TP-LN is described, in the Laplace domain, by its admittance matrix $\mathbf{Y}(s)$. Each entry of $\mathbf{Y}(s)$ is assumed to be a rational function of the complex frequency s.

Step 2) By applying the Mobius transformation technique, we then obtain the admittance matrix $\mathbf{Y}(Z)$ of the TP-LN in the Z-transform domain.

Step 3) Finally, by using appropriate digital-filtering techniques, four sets of first-order difference equations are obtained.

These equations, which describe the *V/I* relation of the TP-LN in the discrete-time domain, are solved in combination with the discrete Maxwell–Ampére's equation. The resulting algorithm preserves the second-order accuracy and the explicit nature of the conventional FDTD method.

To illustrate the validity of the TP-LN-FDTD technique introduced here, we have considered the equivalent circuit of a chip capacitor and a linear circuit model of a generic metal–semiconductor field-effect transistor (MESFET). In the latter case, the intrinsic and extrinsic models of the MESFET are analyzed separately. These three LNs have been placed on a microstrip gap and the scattering parameters of the resulting hybrid circuit have been computed by using the present approach. The results are compared with those obtained by using Agilent Technologies' electromagnetic simulator High Frequency Structure Simulator (HFSS) [19] in combination with the circuital simulator Advanced Design System (ADS) [20], and with those calculated by ADS alone. As the chip capacitor is really a one-port LN, the results for this case are also compared with those computed by using the LN-FDTD method. Experimental measurements have also been carried out for this case.

Manuscript received November 21, 2005; revised March 26, 2006. This work was supported by the Dirección General de Investigación of the Spanish Ministerio de Educación y Ciencia under Project TIC2003–09677–C03–01.

The author are with the Departamento de Ingeniería de Comunicaciones, Universidad de Cantabria, 39005 Santander, Cantabria, Spain (e-mail: pereda@dicom.unican.es).

Digital Object Identifier 10.1109/TMTT.2006.877058

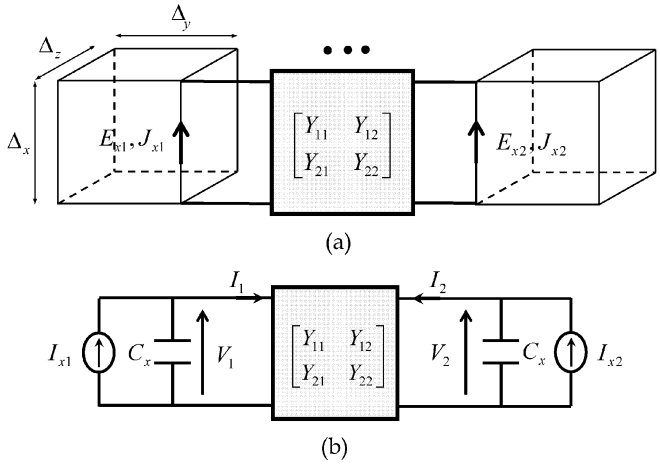

Fig. 1. (a) TP-LN connected to two FDTD unit cells. (b) Equivalent circuit. C_x represents the cell capacitance in the x-direction.

II. Formulation

Consider time-dependent Maxwell's curl equations

$$\mu_0 \partial_t H_\alpha = -[\nabla \times \vec{E}]_\alpha \tag{1a}$$

$$\epsilon \partial_t E_\alpha = [\nabla \times \vec{H}]_\alpha \tag{1b}$$

where $\alpha = x, y, z$. According to the conventional FDTD scheme, the above six equations are expressed in discrete form as

$$H_\alpha^{n+\frac{1}{2}}(\vec{r}_{H_\alpha}) = H_\alpha^{n-\frac{1}{2}}(\vec{r}_{H_\alpha}) - \frac{\Delta_t}{\mu_0}[\nabla \times \vec{E}]_\alpha^n(\vec{r}_{H_\alpha}) \tag{2a}$$

$$E_\alpha^{n+1}(\vec{r}_{E_\alpha}) = E_\alpha^n(\vec{r}_{E_\alpha}) + \frac{\Delta_t}{\epsilon}[\nabla \times \vec{H}]_\alpha^{n+\frac{1}{2}}(\vec{r}_{E_\alpha}) \tag{2b}$$

where $\vec{r}_{E_\alpha}$ and $\vec{r}_{H_\alpha}$ denote the spatial position in the FDTD cell of E_α and H_α, respectively. Explicit expressions for the curl terms can be found, for instance, in [1].

To incorporate a TP-LN into the FDTD formalism, two electrical nodes are used to interface the FDTD mesh with the LN ports. In principle, these nodes neither need to be consecutively located, nor associated to the same component of the electric field. To obtain a more symmetric formulation, however, we consider the LN ports to be associated to the same field component E_{x1} and E_{x2}, as shown in Fig. 1(a). The Maxwell–Ampère's equation, at nodes E_{x1} and E_{x2}, is then complemented by adding a current density term J_{x1} and J_{x2}, respectively. This term is discretized by using a time average; hence, at ports 1 and 2 of the LN, (2b) is replaced by the following equations:

$$E_{x1}^{n+1} = E_{x1}^n + \frac{\Delta_t}{\epsilon}[\nabla \times \vec{H}]_{x1}^{n+\frac{1}{2}} - \frac{\Delta_t}{2\epsilon}\left(J_{x1}^{n+1} + J_{x1}^n\right) \tag{3a}$$

$$E_{x2}^{n+1} = E_{x2}^n + \frac{\Delta_t}{\epsilon}[\nabla \times \vec{H}]_{x2}^{n+\frac{1}{2}} - \frac{\Delta_t}{2\epsilon}\left(J_{x2}^{n+1} + J_{x2}^n\right) \tag{3b}$$

respectively.

The TP-LN is defined in terms of its admittance matrix in the Laplace domain

$$\begin{bmatrix} I_1(s) \\ I_2(s) \end{bmatrix} = \begin{bmatrix} Y_{11}(s) & Y_{12}(s) \\ Y_{21}(s) & Y_{22}(s) \end{bmatrix} \begin{bmatrix} V_1(s) \\ V_2(s) \end{bmatrix} \tag{4}$$

where I_p and $V_p (p = 1, 2)$ are shown in Fig. 1(b). The entries of the admittance matrix are assumed to be rational functions of s as follows:

$$Y_{pq}(s) = \frac{N_{pq}(s)}{D_{pq}(s)} = \frac{\sum_{m=0}^{M_{pq}} a_m^{(p,q)} s^m}{\sum_{m=0}^{M_{pq}} b_m^{(p,q)} s^m} \tag{5}$$

where $a_m^{(p,q)}$ and $b_m^{(p,q)}$ are real-valued coefficients and M_{pq} is the order of the model. It is assumed that, in general, each element of the admittance matrix $Y_{pq}(s)$ has a different model order and a different set of coefficients in the numerator and denominator.

Introducing four auxiliary current intensities $I_{pq}(s)$ (with $p, q = 1, 2$), we express (4) as

$$I_p(s) = \sum_{q=1,2} I_{pq}(s), \qquad p = 1, 2 \tag{6}$$

where

$$I_{pq}(s) = Y_{pq}(s) V_q(s). \tag{7}$$

Notice that the above expression comprises four equations, one for each auxiliary variable $I_{pq}(s)$.

Our goal now is to develop a suitable finite-difference approximation to (6) and (7) in the discrete time domain. Taking the same approach as in [8], we go from the Laplace domain onto the discrete time domain by first passing through the Z-domain.

In the Z-domain, (6) is expressed simply as

$$I_p(Z) = \sum_{q=1,2} I_{pq}(Z), \qquad p = 1, 2 \tag{8}$$

where

$$I_{pq}(Z) = Y_{pq}(Z) V_q(Z) \tag{9}$$

with

$$Y_{pq}(Z) = \frac{\sum_{m=0}^{M_{pq}} c_m^{(p,q)} Z^{-m}}{1 + \sum_{m=1}^{M_{pq}} d_m^{(p,q)} Z^{-m}}. \tag{10}$$

The functions $Y_{pq}(Z)$ are obtained by applying the Mobius transformation,[1] which is given by

$$s = \frac{2}{\Delta_t} \frac{1 - Z^{-1}}{1 + Z^{-1}} \tag{11}$$

[1]This conformal transformation is also known as a "bilinear" or "linear-fractional" transformation.

to $Y_{pq}(s)$ in (5). This transformation preserves the order of the model M_{pq}. The coefficients $c_m^{(p,q)}$ and $d_m^{(p,q)}$ are readily obtained from the time step Δ_t and the coefficients $a_m^{(p,q)}$ and $b_m^{(p,q)}$. This discretization procedure preserves the second-order accuracy of the conventional FDTD method.

Now using the property of the Z-transform $Z^{-m}F(Z) \leftrightarrow F^{n-m}$, (8) and (9) are expressed in the discrete time domain as

$$I_p^{n+1} = \sum_{q=1,2} I_{pq}^{n+1}, \qquad p = 1, 2 \tag{12}$$

and

$$I_{pq}^{n+1} + \sum_{m=1}^{M_{pq}} d_m^{(p,q)} I_{pq}^{n-m+1} = \sum_{m=0}^{M_{pq}} c_m^{(p,q)} V_q^{n-m+1}. \tag{13}$$

By relating, at each port, the voltage with the electric field and the current intensity with the current density as

$$V_p^n = \int E_{xp}^n dx \simeq E_{xp}^n \Delta_x$$
$$I_p^n = \int\int J_{xp}^n \, dy \, dz \simeq J_{xp}^n \Delta_y \Delta_z$$

where $p = 1, 2$, we obtain a field-oriented version of (12) as follows:

$$J_{xp}^{n+1} = \sum_{q=1,2} J_{x,pq}^{n+1}, \qquad p = 1, 2 \tag{14}$$

and (13) as follows:

$$J_{x,pq}^{n+1} + \sum_{m=1}^{M_{pq}} d_m^{(p,q)} J_{x,pq}^{n-m+1} = \sum_{m=0}^{M_{pq}} \bar{c}_m^{(p,q)} E_{xq}^{n-m+1} \tag{15}$$

where

$$\bar{c}_m^{(p,q)} = \frac{\Delta_x}{\Delta_y \Delta_z} c_m^{(p,q)}.$$

The high-order difference equation (15) can be expressed more efficiently as a set of first-order difference equations. To this end, (15) is interpreted as an infinite-impulse response digital filter, which is implemented by using the transpose direct form II as

$$J_{x,pq}^{n+1} = W_{pq,1}^n + \bar{c}_0^{(p,q)} E_{xq}^{n+1} \tag{16a}$$
$$W_{pq,m}^{n+1} = W_{pq,m+1}^n - d_m^{(p,q)} J_{x,pq}^{n+1} + \bar{c}_m^{(p,q)} E_{xq}^{n+1} \tag{16b}$$
$$W_{pq,M_{pq}}^{n+1} = \bar{c}_{M_{pq}}^{(p,q)} E_{xq}^{n+1} - d_{M_{pq}}^{(p,q)} J_{x,pq}^{n+1}. \tag{16c}$$

with $m = 1, 2, \ldots, M_{pq} - 1$. Here, $W_{pq,m}^n (m = 1, \ldots, M_{pq})$ are auxiliary variables and $J_{x,pq}^{n+1}$ is taken as the filter output. In fact, we have four digital filters since $p, q = 1, 2$. Each filter implements one entry of the admittance matrix. Fig. 2 schematically shows the calculation of J_{x1}^{n+1} and J_{x2}^{n+1} from E_{x1}^{n+1} and E_{x2}^{n+1} by using the digital filters (10), implemented by (16), and the output summations (14). The implementation of each individual digital filter is illustrated in Fig. 3.

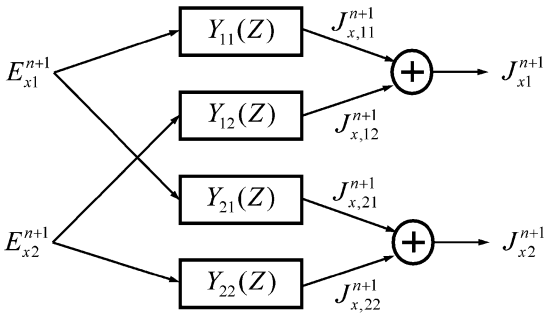

Fig. 2. Calculation of J_{x1}^{n+1} and J_{x2}^{n+1} in terms of E_{x1}^{n+1} and E_{x2}^{n+1}. Each box $Y_{pq}(Z)$ represents a digital filter.

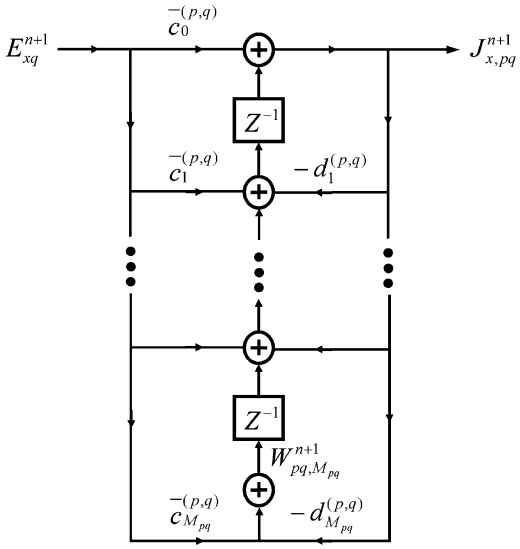

Fig. 3. Implementation of $Y_{pq}(Z)$ by using the transpose direct form II.

Notice that the first equation of each digital filter (16a) is coupled to the Maxwell–Ampère's equation (3). Fortunately, these equations can easily be decoupled before their encoding. Eliminating J_{x1}^{n+1} and J_{x2}^{n+1} from (3) and using (14), we obtain

$$\begin{bmatrix} E_{x1}^{n+1} \\ E_{x2}^{n+1} \end{bmatrix} = \begin{bmatrix} \bar{c}_0^{(1,1)} + \dfrac{2\epsilon}{\Delta_t} & \bar{c}_0^{(1,2)} \\ \bar{c}_0^{(2,1)} & \bar{c}_0^{(2,2)} + \dfrac{2\epsilon}{\Delta_t} \end{bmatrix}^{-1} \begin{bmatrix} T_{x1}^n \\ T_{x2}^n \end{bmatrix} \tag{17}$$

where

$$T_{xp}^n = \frac{2\epsilon}{\Delta_t} E_{xp}^n + 2[\nabla \times \vec{H}]_{xp}^{n+\frac{1}{2}} - \sum_{q=1,2} \left(J_{x,pq}^n + W_{pq,1}^n \right).$$

The matrix inversion that appears in (17) is performed at the preprocessing stage, thus (17) is implemented as a fully explicit expression.

The resulting TP-LN algorithm has the following steps in each time iteration.

Step 1) The magnetic field $\vec{H}^{n+1/2}$, is updated by using the standard FDTD expression (2a).

Step 2) The electric field at the LN ports E_{xp}^{n+1} is updated by using (17).

Step 3) The current densities $J_{x,pq}^{n+1}$ and auxiliary variables $W_{pq,m}^{n+1}$ are updated by using (16), where E_{xq}^{n+1} has been computed in the previous step.

At nodes that are not associated to LN ports, the last two steps are omitted and the electric field is then updated by using the classical FDTD expression (2b).

For the case $Y_{12}(s) = Y_{21}(s) = 0$, the two ports of the TP-LN become mutually decoupled. In this particular situation, the TP-LN-FDTD formulation is reduced to the original LN-FDTD method with one two-terminal LN connected to each port. The two-terminal LN at port 1 is characterized by $Y_{11}(s)$ and the one at port 2 by $Y_{22}(s)$.

III. Validation

To illustrate the validity of the TP-LN-FDTD method described above, we consider the equivalent circuit of a chip capacitor and the linear circuital model of a generic MESFET. In both cases, the device is placed on a microstrip gap and the scattering parameters of the resulting hybrid circuit are computed by the proposed TP-LN-FDTD method.

The microstrip substrate has a dielectric constant $\varepsilon_r = 2.17$ and a thickness $h = 0.254$ mm. The width of the lines is $w = 0.79$ mm, which corresponds to an impedance of approximately 50 Ω. The length of the microstrip gap is $d = 0.5$ mm.

The spatial dimensions of the FDTD cell are $\Delta_x = 0.079$ mm, $\Delta_y = 0.0846$ mm, and $\Delta_z = 0.1$ mm. The time step is $\Delta_t = 0.16$ ps, which corresponds to 0.95$\times$ the maximum time step allowed in the conventional FDTD method. The whole hybrid circuit is enclosed in a perfect electric box of $60 \times 42 \times 175$ cells.

For the examples considered, the results calculated by the TP-LN-FDTD method have been compared with those obtained by combining HFSS with ADS, and with those provided by ADS alone. The approach that combines HFSS with ADS, which will be labeled as HFSS + ADS, consists of first calculating the scattering parameters of the microstrip gap by using HFSS. In this simulation, two additional internal ports are defined. These ports are lumped voltage sources with an internal impedance of 50 Ω. They are located on the gap, each one being connected vertically from the edge of one microstrip line to the ground plane. As a result, a four-port structure is obtained. Once the scattering parameters of this structure have been calculated, the results are exported to a file in CITIfile format and loaded in ADS. The LN is then connected to the internal ports of the gap and the resulting TP hybrid circuit is simulated by ADS.

We consider that the HFSS + ADS approach is more accurate than the use of ADS alone. This is because HFSS provides a fully three-dimensional (3-D) electromagnetic simulation of the microstrip gap. However, according to the ADS documentation, the microstrip gap component, called MGAP, "is an empirically based, analytical model that consists of a lumped component, equivalent circuit. The equivalent circuit parameters are calculated based on the expressions developed by Kirsching, Janse and Koster. Dispersion is included in the capacitance calculation." [21].

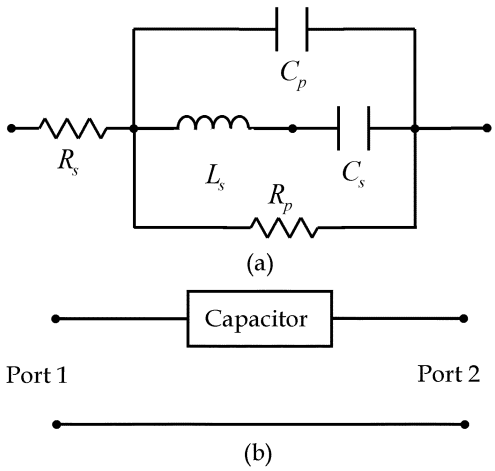

Fig. 4. (a) Equivalent circuit for the G15BU200K5PX05 Gap-Cap capacitor: $L_s = 0.102$ nH, $R_s = 0.139\ \Omega, C_s = 14.93$ pF, $R_p = 268\ \Omega$, $C_p = 5.07$ pF. (b) Capacitor seen as a TP circuit.

A. Chip Capacitor

Fig. 4(a) shows the equivalent circuit of a Gap-Cap capacitor G15BU200K5PX05 [22]. This is a one-port LN, however, it can be also seen as a TP-LN, as shown in Fig. 4(b). The parameters $Y_{pq}(s)$ of the TP model are

$$\begin{aligned} Y_{11}(s) &= \frac{1 + a_1 s + a_2 s^2 + a_3 s^3}{b_0 + b_1 s + b_2 s^2 + b_3 s^3} \\ Y_{12}(s) &= -Y_{11}(s) \\ Y_{21}(s) &= -Y_{11}(s), \\ Y_{22}(s) &= Y_{11}(s) \end{aligned}$$

where $a_1 = (C_p + C_s)R_p, a_2 = L_s C_s, a_3 = R_p L_s C_s C_p, b_0 = R_s + R_p, b_1 = a_1 R_s, b_2 = a_2(R_s + R_p)$, and $b_3 = a_3 R_s$.

The capacitor is connected to the microstrip lines, as illustrated in Fig. 5. It spans five cells, which corresponds to the length of the microstrip gap. Four ideal wires of length Δ_y are used to connect the capacitor to the strips and to the ground plane.

Fig. 6 depicts the magnitude of S_{21} computed by the TP-LN-FDTD method, simulated by ADS and by the HFSS + ADS approach. As the capacitor can also be modeled as a one-port LN, the problem has also been simulated by using the LN-FDTD method. Good agreement is observed among all the simulated results. Fig. 6 also shows measured results that include the effect of two subminiature A (SMA) connectors. Generally speaking, the measured results agree with the simulated ones. The differences observed between simulations and measurements, in the upper part of the frequency band, are mainly due to the influence of the SMA connectors and some mismatching at the ports.

B. MESFET

Firstly, we consider the small-signal equivalent circuit of the intrinsic part of a generic MESFET, as given in [23]. The pa-

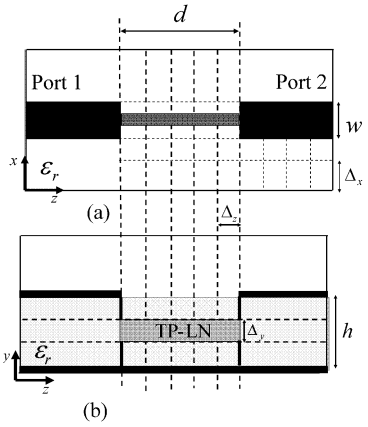

Fig. 5. Simulated hybrid circuit. (a) Top view. (b) Lateral view.

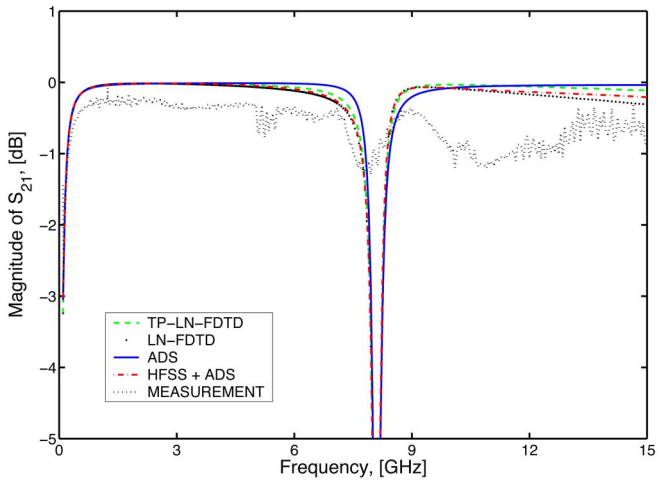

Fig. 6. Magnitude of S_{21} for a Gap-Cap capacitor placed on a microstrip gap. (Color version available online at: http://ieeexplore.ieee.org.)

rameters $Y_{pq}(s)$ of this circuit, which is depicted in Fig. 7, are expressed as

$$Y_{11}(s) = \frac{(C_{\rm gs}+C_{\rm gd})s + C_{\rm gd}C_{\rm gs}R_i s^2}{1+C_{\rm gs}R_i s}$$
$$Y_{12}(s) = -C_{\rm gd}s$$
$$Y_{21}(s) = \frac{G_m - C_{\rm gd}s - C_{\rm gd}C_{\rm gs}R_i s^2}{1+C_{\rm gs}R_i s}$$
$$Y_{22}(s) = G_{\rm ds} + (C_{\rm ds}+C_{\rm gd})s.$$

The transistor is connected to the microstrip lines following the same scheme as that previously described for the capacitor (see Fig. 5).

The magnitude of S_{11} and S_{21} are shown in Figs. 8 and 9, respectively. Three curves can be seen in each figure, which correspond to the TP-LN-FDTD method, the HFSS + ADS approach, and ADS (alone) simulation. Good agreement is observed among these three techniques, although, as expected, the TP-LN-FDTD method provides results that are much closer to those obtained by the HFSS + ADS approach than to those given by ADS.

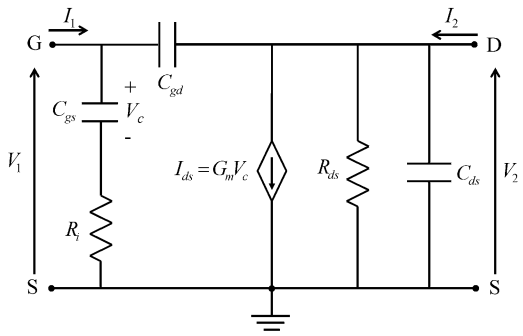

Fig. 7. Intrinsic equivalent circuit for a MESFET with the following parameters: $C_{\rm gd} = 0.06$ pF, $C_{\rm ds} = 0.26$ pF, $C_{\rm gs} = 0.69$ pF, $R_{\rm ds} = 197\ \Omega, G_m = 65$ mS, and $R_i = 1.42\ \Omega$.

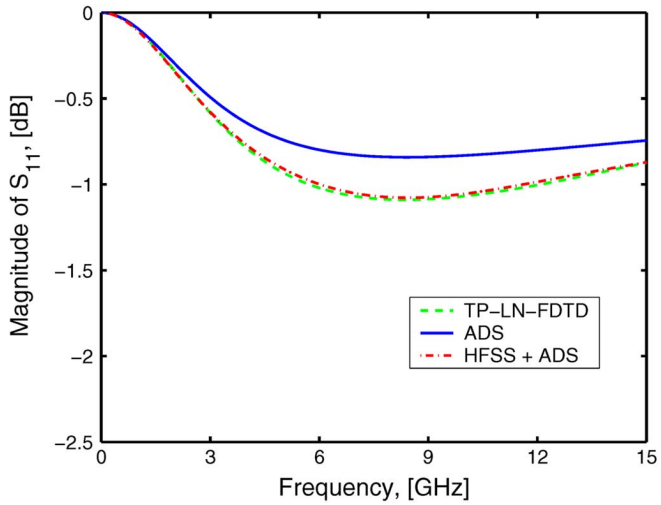

Fig. 8. Magnitude of S_{11} for an intrinsic MESFET mounted on a microstrip gap. (Color version available online at: http://ieeexplore.ieee.org.)

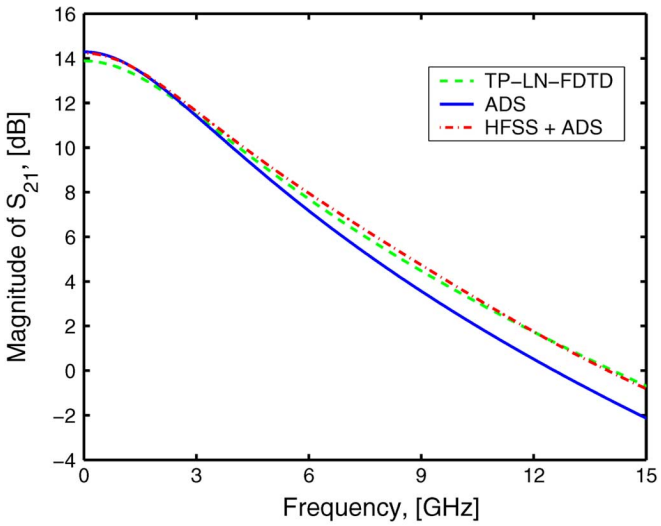

Fig. 9. Magnitude of S_{21} for an intrinsic MESFET on a microstrip gap. (Color version available online at: http://ieeexplore.ieee.org.)

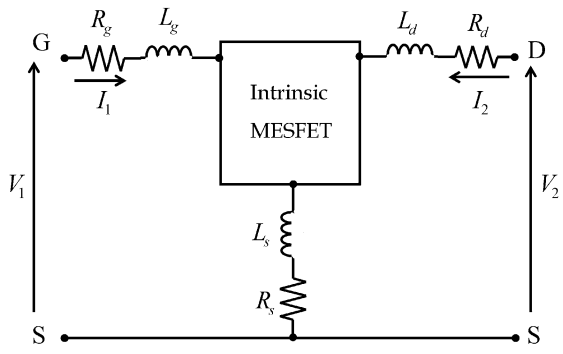

Fig. 10. Extrinsic equivalent circuit for a MESFET with the following parameters: $R_g = 1.39\ \Omega, L_g = 0.37$ nH, $R_d = 1.3\ \Omega, L_d = 0.23$ nH, $R_s = 0.76\ \Omega, L_s = 0.02$ nH. The intrinsic parameters are the same as in Fig. 7.

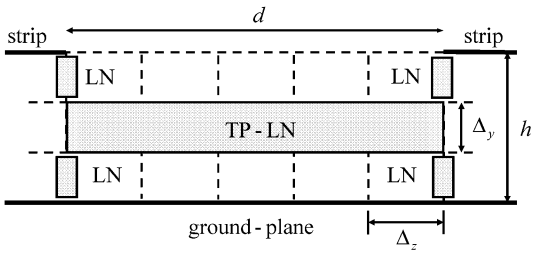

Fig. 11. FDTD model of the MESFET, shown in Fig. 10 mounted on a microstrip gap.

Secondly, we consider the equivalent circuit of a generic MESFET including both its intrinsic and extrinsic parts, as shown in Fig. 10.

This circuit can be incorporated into a FDTD simulation by following the TP-LN-FDTD technique, as was done previously when the intrinsic part of the transistor was considered alone. However, the order of the resulting admittance parameters is high (larger than ten), which means that time derivatives of the same order must be discretized. Also, in the TP-LN-FDTD method, each port occupies just one cell, thus wires are needed to connect the MESFET to the strips and to the ground plane. Taking these aspects into account, we thought that a better choice would be an approach that combines the TP-LN-FDTD and the LN-FDTD methods. The intrinsic part of the MESFET is modeled by the TP-LN-FDTD method and the extrinsic part by the LN-FDTD technique. The connection scheme is shown in Fig. 11. To avoid the use of connecting wires and to maintain symmetry, the series L_sR_s of the source terminal, shown in Fig. 10, is split into two equal LNs. By using this approach, the highest time derivative involved is only of second order.

The results for the magnitude of S_{11} and S_{21} are shown in Figs. 12 and 13, respectively. The same comments made for the results of the intrinsic MESFET can be repeated here, with the remark that, in this case, the difference between the curves for S_{11} obtained by the TP-LN-FDTD method and by the HFSS + ADS approach is a bit greater than in the case of the intrinsic MESFET.

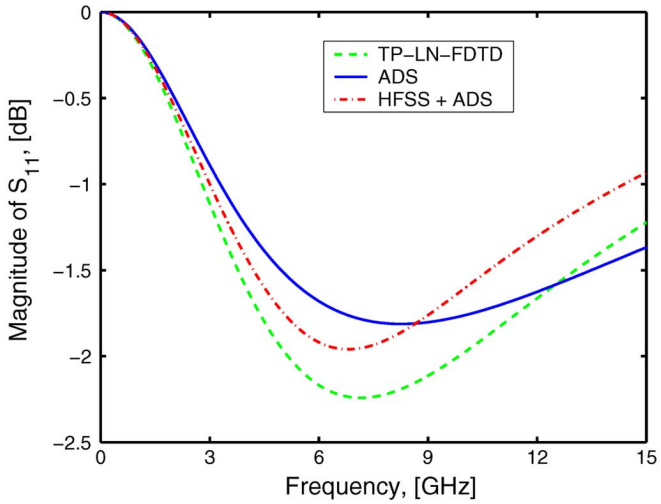

Fig. 12. Magnitude of S_{11} for an extrinsic MESFET mounted on a microstrip gap. (Color version available online at: http://ieeexplore.ieee.org.)

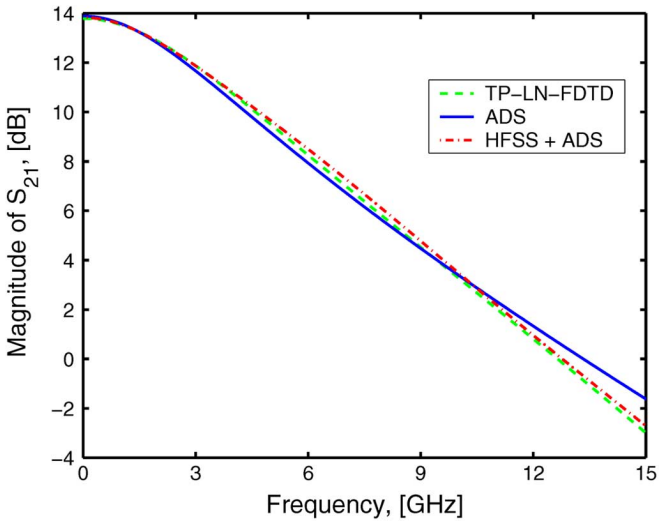

Fig. 13. Magnitude of S_{21} for an extrinsic MESFET mounted on a microstrip gap. (Color version available online at: http://ieeexplore.ieee.org.)

IV. Conclusion

This paper has extended the LN-FDTD method to linear TP-LNs. To this end, the LN is described by its admittance matrix $\mathbf{Y}(s)$ in the Laplace domain. The entries of $\mathbf{Y}(s)$ are assumed to be rational functions of s. By applying the Mobius transformation technique to $\mathbf{Y}(s)$, we obtain the admittance matrix in the Z-transform domain. Appropriate digital-filtering techniques are then used to obtain four sets of first-order finite-difference equations, which describe the *V/I* relation of the LN in the discrete time domain. The resulting algorithm preserves the second-order accuracy and the explicit nature of the conventional FDTD method. The validity of this new formulation has been demonstrated by computing the scattering parameters of several hybrid circuits.

Wave digital filters can be used as an alternative to the digital filters employed in this paper [24].

REFERENCES

[1] A. Taflove and S. Hagness, *Computational Electrodynamics: The Finite-Difference Time-Domain Method*, 2nd ed. Boston, MA: Artech House, 2000.

[2] W. Sui, D. A. Chistensen, and C. H. Durney, "Extending the two-dimensional FDTD method to hybrid electromagnetic systems with active and passive lumped elements," *IEEE Trans. Microw. Theory Tech.*, vol. 40, no. 4, pp. 724–730, Apr. 1992.

[3] Y.-S. Tsuei, A. C. Cangellaris, and J. L. Prince, "Rigorous electromagnetic modeling of chip-to-package (first-level) interconnections," *IEEE Trans. Compon., Hybrids, Manuf. Technol.*, vol. 16, no. 8, pp. 876–883, Aug. 1993.

[4] M. Piket-May, A. Taflove, and J. Baron, "FD-TD modeling of digital signal propagation in 3-D circuits with passive and active loads," *IEEE Trans. Microw. Theory Tech.*, vol. 42, no. 8, pp. 1514–1532, Aug. 1994.

[5] C.-N. Kuo, V. A. Thomas, S. T. Chew, B. Houshmand, and T. Itoh, "Small-signal analysis of active circuits using FDTD algorithm," *IEEE Microw. Guided Wave Lett.*, vol. 5, no. 7, pp. 216–218, Jul. 1995.

[6] P. Ciampolini, P. Mezzanotte, L. Roselli, and R. Sorrentino, "Accurate and efficient circuit simulation with lumped-element FDTD technique," *IEEE Trans. Microw. Theory Tech.*, vol. 44, no. 12, pp. 2207–2215, Dec. 1996.

[7] X. Ye and J. L. Drewniak, "Incorporating two-port networks with S-parameters into FDTD," *IEEE Microw. Wireless Compon. Lett.*, vol. 11, no. 2, pp. 77–79, Feb. 2001.

[8] J. A. Pereda, F. Alimenti, P. Mezzanotte, L. Roselli, and R. Sorrentino, "A new algorithm for the incorporation of arbitrary linear lumped networks into FDTD simulators," *IEEE Trans. Microw. Theory Tech.*, vol. 47, no. 6, pp. 943–949, Jun. 1999.

[9] J. W. Schuster, R. J. Luebbers, and T. G. Livernois, "Application of the recursive convolution technique to modeling lumped-circuit elements in FDTD simulations," in *Proc. IEEE Int. AP-S Symp.*, 1998, vol. 4, pp. 1792–1795.

[10] W. Yuan and E. Li, "FDTD simulations for hybrid circuits with linear and nonlinear lumped elements," *Microw. Opt. Technol. Lett.*, vol. 32, no. 6, pp. 408–412, Mar. 2002.

[11] T.-L. Wu, S.-T. Chen, and Y.-S. Huang, "A novel approach for the incorporation of arbitrary linear lumped networks into FDTD method," *IEEE Microw. Wireless Compon. Lett.*, vol. 14, no. 2, pp. 74–76, Feb. 2004.

[12] H. E. Abd El-Raouf, W. Yu, and R. Mittra, "Application of the Z-transform technique to modelling linear lumped loads in the FDTD," *Proc. Inst. Elect. Eng.—Microw. Antennas Propag.*, vol. 151, no. 1, pp. 67–70, Feb. 2004.

[13] Z. H. Shao and M. Fujise, "An improved FDTD formulation for general linear lumped microwave circuits based on matrix theory," *IEEE Trans. Microw. Theory Tech.*, vol. 53, no. 7, pp. 2261–2266, Jul. 2005.

[14] J.-Y. Lee, J.-H. Lee, and H.-K. Jung, "Modeling linear lumped loads in the FDTD method using piecewise linear recursive convolution method," in *Proc. IEEE AP-S Int. Symp.*, 2005, vol. 2B, pp. 142–145.

[15] G. Emili, F. Alimenti, P. Mezzanotte, L. Roselli, and R. Sorrentino, "Rigorous modeling of packaged Schottky diodes by the nonlinear lumped network (NL^2N)-FDTD approach," *IEEE Trans. Microw. Theory Tech.*, vol. 48, no. 12, pp. 2277–2282, Jan. 2000.

[16] O. El Mrabet and M. Essaaidi, "Comments on 'Rigorous modeling of packaged Schottky diodes by the nonlinear lumped network (NL^2N)-FDTD approach'," *IEEE Trans. Microw. Theory Tech.*, vol. 50, no. 12, pp. 2411–2412, Oct. 2002.

[17] G. Emili, F. Alimenti, P. Mezzanotte, L. Roselli, and R. Sorrentino, "Authors' reply," *IEEE Trans. Microw. Theory Tech.*, vol. 50, no. 10, p. 2412, Oct. 2002.

[18] O. El Mrabet and M. Essaaidi, "An efficient algorithm for the global modeling of RF and microwave circuits using a reduced nonlinear lumped network (RNL^2N)-FDTD approach," *IEEE Microw. Wireless Compon. Lett.*, vol. 14, no. 2, pp. 86–88, Feb. 2004.

[19] High Frequency Structure Simulator 5.6. Agilent Technol., Palo Alto, CA, 2000.

[20] Advanced Design System 2005A. Agilent Technol., Palo Alto, CA, 2005.

[21] M. Kirschning, R. H. Jansen, and N. H. L. Koster, "Measurement and computer aid modeling of microstrip discontinuities by an improved resonator method," *IEEE MTT-S Int. Microw. Symp. Dig.*, pp. 495–497, May 1983.

[22] Cap Cad. ver. 3.0.2, Dielectrics Labs. Inc., Cazenovia, NY, 2000 [Online]. Available: http://www.dilabs.com

[23] P. H. Ladbrooke, *MMIC Design: GaAs FETs and HEMTs*. Norwood, MA: Artech House, 1989.

[24] A. Fettweis, "Multidimensional wave digital filters for discrete-time modelling of Maxwell's equations," *Int. J. Numer. Modeling*, vol. 5, pp. 183–201, Aug. 1992.

Oscar González was born in Santander, Spain, in 1978. He received the Telecommunications Engineering degree from the Universidad de Cantabria, Santander, Cantabria, Spain, in 2002, and is currently working toward the Ph.D. in telecommunications engineering at the Universidad de Cantabria.

His research interests include numerical methods in electromagnetics, characterization of electromagnetic properties of materials, and microwave devices.

José A. Pereda (S'93–M'95) was born in Madrid, Spain, in 1966. He received the Licenciado and Ph.D. degrees in physics from the Universidad de Cantabria, Santander, Cantabria, Spain, in 1989 and 1995, respectively.

In 1989, he joined the Electronics Department, Universidad de Cantabria. From 1996 to 2001, he was an Assistant Professor with the Departamento de Ingeniería de Comunicaciones, Universidad de Cantabria, and in 2001, he became an Associate Professor in electromagnetism. His research interests include electromagnetic-field theory and numerical methods for solving electromagnetic problems.

Amparo Herrera (M'06) was born in Aviles (Asturias), Spain. She received the Electronic Physics and Ph.D. degrees from the Universidad de Cantabria, Santander, Spain, in 1987 and 1995, respectively.

In 1987, she joined the CIDA (Spanish Navy, Research and Development (R&D) Centre), where she was in charge of the development of its RF laboratories and the supervision of several Spanish R&D projects. In 1990, she joined the Universidad de Cantabria, where she was involved in RF monolithic-microwave integrated-circuit (MMIC) design. During this period, she designed (in 1992) several MMIC power amplifiers for Philips Microwave Limeil (PML) (now OMMIC). Since 1996, she has been an Associate Professor (permanent since March 2003) with the Departamento de Ingeniería de Comunicaciones, Universidad de Cantabria. Her areas of interest include hybrid and MMIC design of RF and microwave circuits and integration of communication systems. In particular, she is the researcher responsible for Spanish National projects related to the MMIC design for satellite on-board systems.

Ángel Vegas (M'98) was born in Santander, Spain. He received the Licenciado degree in physics and Ph.D. degree from the Universidad de Cantabria, Santander, Cantabria, Spain, in 1976 and 1983, respectively.

From 1977 to 1983, he was with the Department of Electronics, Universidad de Cantabria, where he became an Associate Professor in 1984. He has been involved with electromagnetic wave propagation in plasmas and microwave interferometry. His current research and teaching interests include electromagnetic theory, computer methods in electromagnetism, and microwave measurements.